Available online at www.sciencedirect.com
SCIENCE DIRECT®
Journal of volcanology and geothermal research
ELSEVIER
Journal of Volcanology and Geothermal Research xx (2005) xxx–xxx
www.elsevier.com/locate/jvolgeores

An increment of volcano collapse: Kinematics of the 1975 Kalapana, Hawaii, earthquake

Susan E. Owen [a,*], Roland Bürgmann [b]

[a] *Department of Earth Sciences, University of Southern California, Los Angeles, California, 90089-0742, United States*
[b] *University of California-Berkeley, Department of Geology and Geophysics, 375 McCone Hall, Berkeley, California, 94720-4767, United States*

Received 4 June 2004; received in revised form 5 October 2004

Abstract

Earthquakes on Kilauea Volcano can be even more hazardous than volcanic eruptions. The most recent large earthquake was the 1975 Kalapana quake, which generated a locally damaging tsunami, over 8 m of horizontal surface displacement and 3 m of subsidence at the coast. The seismic magnitude estimates for this earthquake range from Ms 7.2 to Mw 7.7. The complexity of the seismic data is matched by the complex surface deformation that was observed with a combination of leveling, tilt and Electronic Distance Measurements (EDM). The geodetic data shows evidence of collapse of the caldera due to magma withdrawal, localized subsidence over the rift zone, normal faulting associated with shallow slumping along the Hilina Pali, and displacement on the basal detachment fault. We model the summit caldera, rift zones and basal detachment fault as dislocations in an elastic half-space to better quantify the sources of deformation related to this devastating event. Using inversion techniques that allow us to let the data constrain the geometry and magnitude of these sources, we find 0.04 km^3 of magma withdrawal at the summit, between 3–5 m of opening along the rift zone and 7.1 m of slip along the basal detachment at 8.3 km depth. Models that allow for finer spatial resolution of slip on the detachment show that the largest slip occurred west of the seismically recorded earthquake hypocenter, along the region of the fault below the coast, and that the majority of the fault slip occurred south of the region of microseismicity. Our best-fitting model has a geodetic moment of 4.1×10^{20} Nm (M_w 7.7), which is consistent with tsunami models and recent analysis of long period seismic data. The residual displacements of sites located in the hanging wall of the Hilina Pali slump system, which were not used in the inversion of the other sources, suggest that triggered shallow slumping contributed several meters of horizontal displacement to the coseismic displacement at these sites.

Keywords: Kilauea; volcanoes; earthquakes; rift zones; geodesy; trilateration; leveling; tilt

* Corresponding author. Tel.: +1 213 740 6308; fax: +1 213 740 8801.
E-mail addresses: owen@usc.edu (S.E. Owen), burgmann@seismo.berkeley.edu (R. Bürgmann).

0377-0273/$ - see front matter © 2005 Elsevier B.V. All rights reserved.
doi:10.1016/j.jvolgeores.2005.07.012

1. Introduction

The active volcanoes of Hawaii are responsible for recurrent damaging earthquakes, the most recent being the events of 1975 and 1989. Both earthquakes occurred beneath the structurally unstable south flank of Kilauea Volcano, but also caused internal deformation of the south flank block and magma redistribution. Other volcanic flanks, especially those on oceanic shields, exhibit evidence for slumping and catastrophic gravity sliding during their growth. Benefiting from the dense seismometer network and rich geodetic database collected by the Hawaiian Volcano Observatory (HVO) (Lipman et al., 1985), we evaluate kinematic models of the 1975 Kalapana earthquake deformation to improve our understanding of the processes that cause large volcanic edifices to fail. We hope to better understand the seismic hazard of Kilauea's south flank through rigorous analysis of geodetic data spanning this largest Hawaiian earthquake of the past century.

2. Hawaiian earthquakes and Kilauea's edifice structure

The south flank of Kilauea Volcano, Hawaii, experienced significant historic earthquakes ($M>6$) in 1823, 1868, 1954, 1975, and 1989 (Fig. 1) (Wyss and Koyanagi, 1992a). These earthquakes caused significant damage with strong shaking, landsliding, coastal subsidence, and destructive tsunamis. Seismic, geodetic and tsunami data reveal that the 1975 $M_s=7.2$ earthquake (Ando, 1979; Lipman et al., 1985; Tilling et al., 1976) and the 1989 $M_s=6.1$ earthquake (Arnadottir et al., 1991; Bryan and Johnson, 1991) occurred primarily on sub-horizontal thrust faults near the base of the volcanic edifice at about 8–10 km depth (Fig. 1A,B) (Ando, 1979; Arnadottir et al., 1991; Crosson and Endo, 1982; Furumoto and Kovach, 1979; Hill and Zucca, 1987; Lipman et al., 1985). Coastal subsidence patterns and local tsunami heights during the $M \approx 8$ 1868 Kau earthquake resembled those of 1975 and suggest basal detachment below Kilauea as well as Mauna Loa (Ando, 1979; Hitchcock, 1912; Wood, 1914; Wyss, 1988).

The south flank of Kilauea is defined as the portion of the island of Hawaii that lies south of Kilauea's summit and rift zones. This region has been displaced seaward by magmatic intrusions, gravitational spreading of hot dense rock within the deep rift system and slip on the basal detachment fault (Clague and Denlinger, 1994; Crosson and Endo, 1982; Delaney et al., 1990; Denlinger and Okubo, 1995; Dieterich, 1988; Harvey and Wyss, 1986; Lipman et al., 1985; Ryan, 1988; Swanson et al., 1976; Thurber and Gripp, 1988). Detachment faulting and

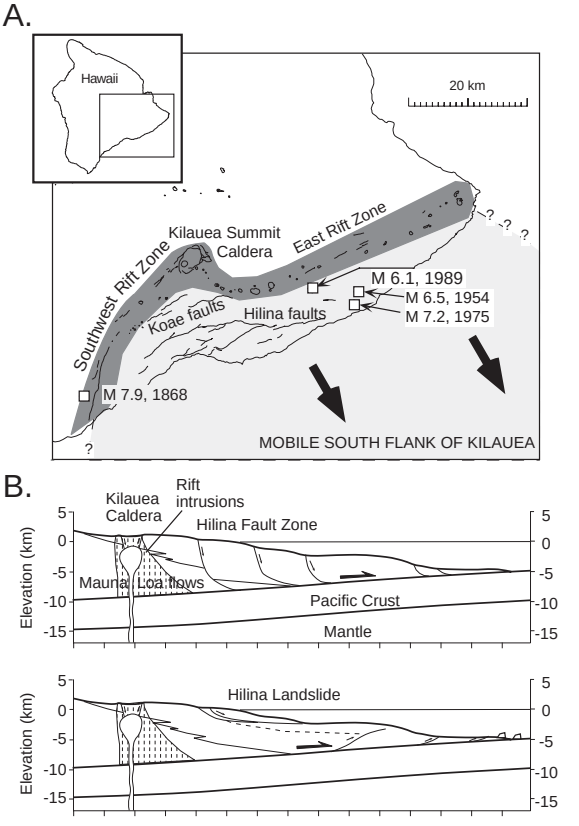

Fig. 1. (A) Location map of Kilauea's south flank. Historic $M>6$ earthquake epicenters are labeled with their magnitude and year. (B) Cross-sections across Kilauea's south flank showing two general interpretations proposed for the subsurface structure of the Hilina fault zone (based on Lipman et al., 1985; Hill and Zucca, 1987; and Morgan et al., 2003). The depth and dip of the Pacific plate, the inferred dike complex below the volcanic rift zones, and the stratigraphy of the south flank are based on gravity and seismic refraction data reviewed by Hill and Zucca (1987). A deeply rooted Hilina fault system is supported by microseismicity and seismic tomography results (Okubo et al., 1997). A shallow system, soling out at 2–4 km depth, is consistent with the surface geometry and offshore seismic reflection data (Cannon et al., 2001; Morgan et al., 2003).

volcanic activity are evidently linked through the long-term accommodation of rift-system magma and cumulate by the southward motion of the south flank (Delaney et al., 1990, 1993; Dieterich, 1988; Hill and Zucca, 1987; Owen et al., 1995, 2000; Swanson et al., 1976). The formation of a broad dike complex (~10-km-wide at its base) along the rift zones of Kilauea (Hill and Zucca, 1987) and a wide deformation zone offshore of Hawaii (Morgan et al., 2000) suggest that the seaward motion of the south flank has occurred over a long time period. Large normal fault scarps of the Hilina fault zone (Hilina Palis) on the slopes of Kilauea suggest that gravitational forces play an important role in the internal deformation of the south flank (Dieterich, 1988). The whole south flank has been likened to a large landslide block that may fail catastrophically, as has happened previously on the Hawaiian islands (Denlinger and Okubo, 1995; Lipman et al., 1988; Moore and Chadwick, 1995; Moore and Moore, 1984; Moore et al., 1994).

The Hilina fault system forms impressive south-facing normal fault scarps of up to 500-m relief (Fig. 2), creating dramatic cliffs that are called "palis" in Hawaiian. The Hilina Pali stretch for ~40 km along the south flank of Kilauea (Cannon et al., 2001; Kellogg and Chadwick, 1987; Lipman et al., 1985). Some consider the Hilina fault zone to be a shallow landslide structure that experiences triggered slip during large earthquakes (Fig. 1b bottom) (Cannon et al., 2001; Hill and Zucca, 1987; Stearns and Macdonald, 1946; Swanson et al., 1976). Alternatively, the Hilina faults may root into the basal detachment and play an important role in the active deformation of the south flank block (Fig. 1b top) (Denlinger and Okubo, 1995; Lipman et al., 1985; Moore and Chadwick, 1995; Okubo et al., 1997). The Hilina Pali fault system slipped 1–3 m along a 25-km-long segment during the 1975 event. Although the Hilina faults did not slip during the 1989 earthquake that ruptured eastward from its hypocenter (Fig. 1), there was ground breakage along the north-facing Hakuma normal fault that forms part of a horst-and-graben system seaward of the Hilina faults (Delaney et al., 1993). Slip, although less than a meter, along this coastal fault attests to triggering of subsidiary faults during the deeper, decollement-type events.

Much of our knowledge about the active tectonics of Kilauea comes from geodetic studies. Historic deformation measurements on the south flank were collected since the late 19th century and span a large number of rift intrusion events and two large earthquakes. It is generally thought that magma accumulation and creep within the rift system, together with gravitational forces, deform the south flank and cause detachment earthquakes (Delaney et al., 1993; Dieterich, 1988; Dvorak, 1986; Lipman et al., 1985; Swanson et al., 1976; Wyss et al., 1981). Eighty years of triangulation and trilateration measurements provide a record of strain accumulation before the 1975 earthquake (Swanson et al., 1976). Up to 2 m of contraction across the subaerial south flank was inferred in the 80 yr preceding the 1975 earthquake, leading to speculations about an impending rupture just before the event (Swanson et al., 1976). It is not clear if these pre-earthquake displacements were caused solely by magma emplacement into Kilauea's southwest and east rift zones, or if there was some concurrent basal fault slip preceding the 1975 earthquake (Delaney et al., 1992).

Trilateration data and GPS (Global Positioning System) measurements collected since 1975 observe rapid surface displacement rates of about 10 cm/yr that are consistent with the basal detachment fault beneath Kilauea's south flank slipping at a rate of 10–20 cm/yr, and concurrent rift opening at comparable rates (Delaney et al., 1998, 1990, 1993; Owen et al., 1995, 2000). That is, the deformation is characterized by continued aseismic motion on and adjacent to the coseismic rupture plane with little evidence for renewed elastic strain accumulation about a locked fault plane. There is no evidence for noticeable slip on the Hilina fault system since the 1975 earthquake (Delaney et al., 1998; Owen et al., 2000).

2.1. The 1975 Kalapana earthquake

The 29 November 1975 Kalapana earthquake was preceded by several foreshocks that are distributed across a several-km-wide zone (Fig. 3). The largest, $M \approx 5.7$, occurred about 3 km north of the mainshock epicenter. Focal mechanisms of the largest foreshock and the mainshock have ~N55°-60°E striking, subvertical and sub-horizontal nodal planes, approximately parallel to Kilauea's rift system and the Hilina

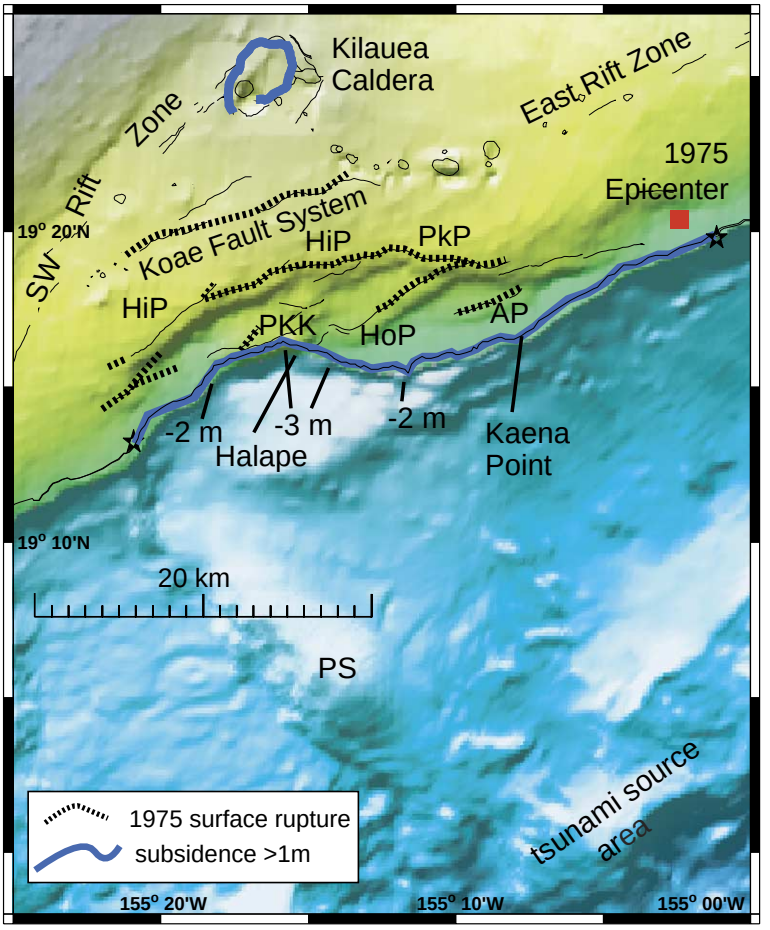

Fig. 2. Ground deformation from the 1975 Kalapana earthquake including coastal subsidence (subsidence was >1 m between stars, based on Lipman et al., 1985), Hilina fault slip (based on Lipman et al., 1985; Kellogg and Chadwick, 1987; and Cannon et al., 2001), fracturing and extension along Koae fault zone (Lipman et al., 1985; and J. Lockwood, personal fieldnotes); and the center of tsunami-generating offshore uplift near the toe of the south flank wedge (from Ma et al., 1999). Note offshore morphology showing closed basins bounded seaward by an elevated bench and the irregular shaped toe of the slump. Seismic reflection data of Morgan et al. (2000, 2003) suggests that this morphology represents thrusts splaying off the basal detachment and individual landslide blocks. PS, Papa'u "seamount"; HiP, Hilina Pali; PKK, Puu Kapukapu; HoP, Holei Pali; PkP, Poliokeawe Pali; AP, Apua Pali.

fault system. Based on considerations of event magnitude, tsunami and geodetic data, and aftershock distribution, the mainshock active nodal plane was determined to be sub-horizontal (Ando, 1979; Crosson and Endo, 1981; Furumoto and Kovach, 1979; Harvey and Wyss, 1986; Ma et al., 1999; Nettles and Ekstrom, 2004). Eissler and Kanamori (1987) argue for a near-horizontal single force (slump) mechanism based on an analysis of surface wave data (see also Wyss, 1988). The rupture propagated ~45 km westward in at least 6 sub-events for about 50 s along the detachment surface at 8–10 km depth (Harvey and Wyss, 1986). The downdip width of the rupture was initially estimated to be about 20 km (Ando, 1979). Early estimates suggest that the event had a seismic moment of $1.2-1.8\times10^{20}$ Nm and an average SSE-directed slip of 3.75–5.5 m (Ando, 1979; Crosson and Endo, 1981). The estimated source area and magnitude of the associated tsunami suggest an event significantly larger than

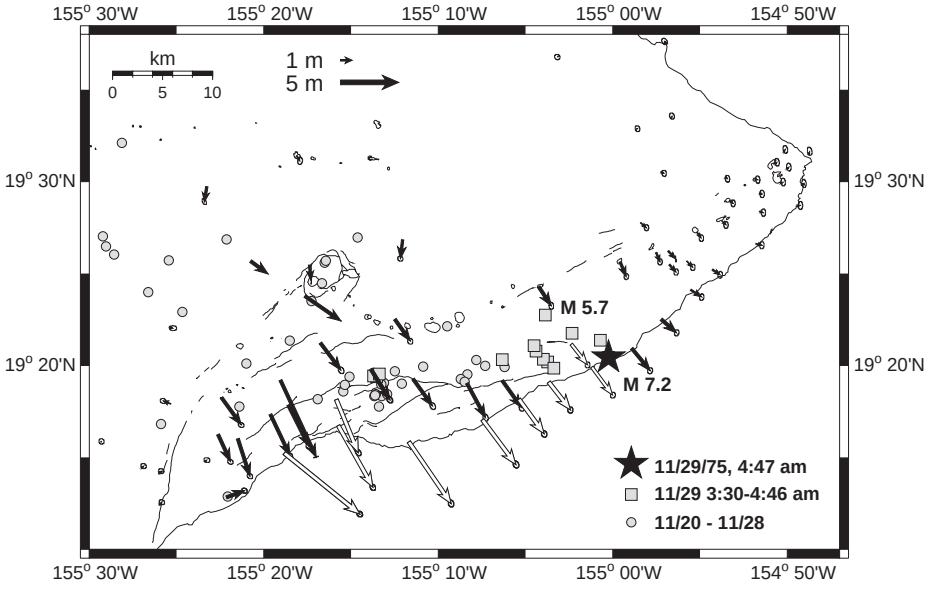

Fig. 3. Horizontal displacements associated with the Kalapana earthquake deduced from trilateration measurements. Displacements and 95% confidence ellipses computed using a model coordinate solution (Segall and Mathews, 1988) of the line-length data. No stations are held fixed in this solution, and network rotations and translations are minimized relative to displacements from a dislocation model inverted from the combined data set of trilateration, leveling, and tilt data. Note that the largest displacements occur at sites in the hanging wall of the Hilina faults and north of a distinct topographic bench apparent in the bathymetry of the south flank (Fig. 2). Displacements of stations shown as open arrows are not included in the inversions for coseismic detachment slip (Figs. 8–10). The black star indicates the Kalapana earthquake epicenter, the gray-shaded squares and circles indicate earthquakes which occurred in the hour or week preceding the event, respectively.

indicated by the seismic moment (Ando, 1979; Ma et al., 1991). Ma et al. (1999) find that the tsunami data are best fit by a propagating slump model with about 1 m subsidence near the coast and 1 m uplift ~30 km offshore (Fig. 2) displacing about 2.5 km^3 of water. Alternatively, they suggest that slip on a deep detachment, that reaches out to the toe of the south flank system, may fit the data equally well. Most recently Nettles and Ekstrom (2004) performed a careful reanalysis of the long period surface waves and find a significantly larger seismic moment, 3.81×10^{20} Nm. They find that the rupture process for the Kalapana earthquake was very slow, lasting for 72 s instead of the expected ~34 s. Their estimated earthquake centroid is located seaward of the point where rupture initiated. This centroid location indicates that the earthquake likely propagated into the offshore part of the fault, consistent with the wide-detachment model of Ma et al. (1999).

Significant ground deformation occurred in the form of seaward displacement, coastal subsidence, offshore uplift, normal slip along the Hilina fault system, distributed fracturing along the Koae fault system, and collapse of the Kilauea caldera (Figs. 2, 3) (Lipman et al., 1985; Tilling et al., 1976). Coastal subsidence exceeded 1 m along a >30-km-long zone, with subsidence approaching 3.5 m near Halape (Lipman et al., 1985). During the event normal faulting occurred along multiple strands of the Hilina fault system from about 7 to 32 km west of the epicenter (Lipman et al., 1985). Coseismic offsets of up to 3 m can be observed along the central Poliokeawe and Holei Palis (Bürgmann and Denlinger, 1995; Cannon et al., 2001; Kellogg and Chadwick, 1987). If steep normal faulting continued to greater depth, Hilina slip of 1–3 m could account for about two-thirds of the coastal subsidence along Kilauea's south coast (Lipman et al., 1985). The geodetically measured ground deformation is described below; a detailed analysis of the coseismic surface offsets along the Hilina faults is presented by Cannon et al. (2001).

Most aftershocks of the 1975 earthquake, and the majority of microseismicity overall, are restricted to the 5–10 km-wide zone, bordered by the Kilauea rift zones to the north and west, and by the surface trace of the Hilina fault zone to the south (Klein et al., 1987; Lipman et al., 1985). The aftershock sequence decayed slowly in the following years, punctuated by rift intrusions and the 1989 earthquake (Delaney et al., 1993; Klein et al., 1987). The majority of the south flank microseismicity since the decay of the aftershock sequence has also been restricted to the same 5–10 km wide zone.

3. Geodetic measurements of Kilauea deformation

To develop a model of coseismic deformation during the Kalapana earthquake, we need to establish a data set of geodetic measurements that is little affected by other deformation sources. In addition to recurrent cycles of summit inflation and deflation that accompany dike intrusions and, often, eruptions, Kilauea undergoes approximately continuous extension along much of its rift system. The area of most rapid extension, the summit, was extending about 20 cm/yr for several years prior to the earthquake and more than 25 cm/yr for several years afterward (Delaney et al., 1998; Swanson et al., 1976).

Despite frequent geodetic monitoring, several factors mitigate against the creation of a complete and purely coseismic data set. First of all, the earthquake deformed much of the volcano but the most intense geodetic coverage is around the summit and upper rift zones. Secondly, the preseismic and postseismic leveling, trilateration, and ground-surface tilt measurement intervals are not the same, nor is the frequency of measurements the same at all stations. Thus the data include various amounts of pre- and post-earthquake deformation, which are difficult to isolate. Thirdly, a large seismic swarm and moderate eruption along the southwest rift zone on 31 December 1974 interrupted the 1974 Kilauea trilateration survey and the network was not entirely reoccupied afterwards. Finally, postseismic displacements were large and most of the measurement methods at the time were not operating in a continuous mode. Several kilometer-long level sections, for instance, underwent 100-μrad tilts during the first six months after the earthquake. Delaney et al. (1990) found that estimated heights of certain benchmarks at the distal southeast end of the Kilauea leveling network varied by 20 cm with selection of particular post-seismic data.

Fig. 4 shows the occupation times utilized in this study superimposed on a continuous record of summit deformation: the north component of water tube tilt observations at Uwekahuna located just northwest of Kilauea caldera. A histogram shows the number of

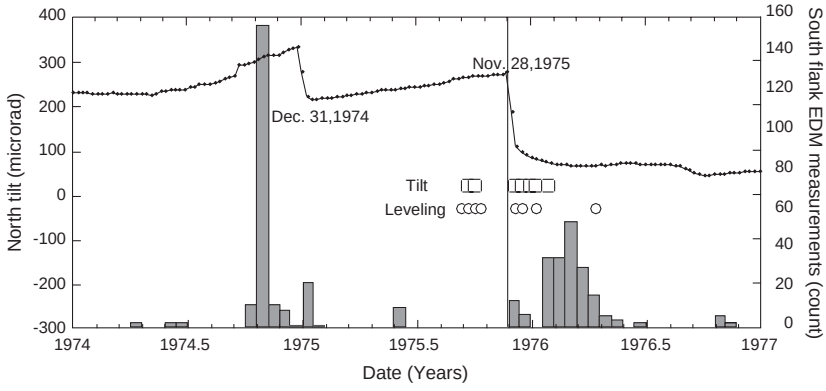

Fig. 4. Geodetic measurements used to constrain the deformation associated with the Kalapana earthquake. Small circles show the north tilt history at Uwekahuna on the north rim of the summit caldera for reference (Fig. 5). Tilt measurements (open squares) and the level measurements used here (open circles) were conducted within a few months before and after the earthquake. The histogram shows the number of line-length measurements between sites of the regional south flank network. Not included are the more often repeated (at least every two months) occupations of the summit network.

trilateration baseline measurements in the regional south flank network. It is apparent that only a limited number of baselines were remeasured between the 31 December 1974 rift intrusion and the Kalapana earthquake, thus necessitating the more detailed consideration of the rift intrusion deformation described below. The summit network was measured at least every two months and some summit sites were occupied daily immediately following the event. In our effort to produce an adequate representation of coseismic deformation, we utilize data with the shortest time span that includes the earthquake, and correct for the effects of the 31 December 1974 southwest rift intrusion.

3.1. Leveling measurements of vertical displacements

Level lines are occupied at very irregular intervals, with the coseismic measurement intervals ranging from several months to more than 10 yr (Lipman et al., 1985). Fortunately, leveling near Kilauea summit was completed several months before the earthquake and was remeasured expeditiously afterwards. Unfortunately, level sections across the south flank and lower east rift zone span longer time periods. We do not use >10-yr-old data spanning the lower east rift zone (Lipman et al., 1985), as these might be dominated by deformation associated with long-term rift opening. Although the coseismic leveling measurements are likely affected by significant postseismic deformation, we do not attempt to remove the postseismic deformation from the elevation changes used to compute our models. All elevation changes were recomputed from files archived at HVO.

Relative to a local datum near a tide gage in Hilo (Benchmark A100), all benchmarks experienced subsidence during the 1975 earthquake (Fig. 5; (Lipman et al., 1985)). The summit caldera subsided as much as 1.5 m, with subsidence extending along the south-

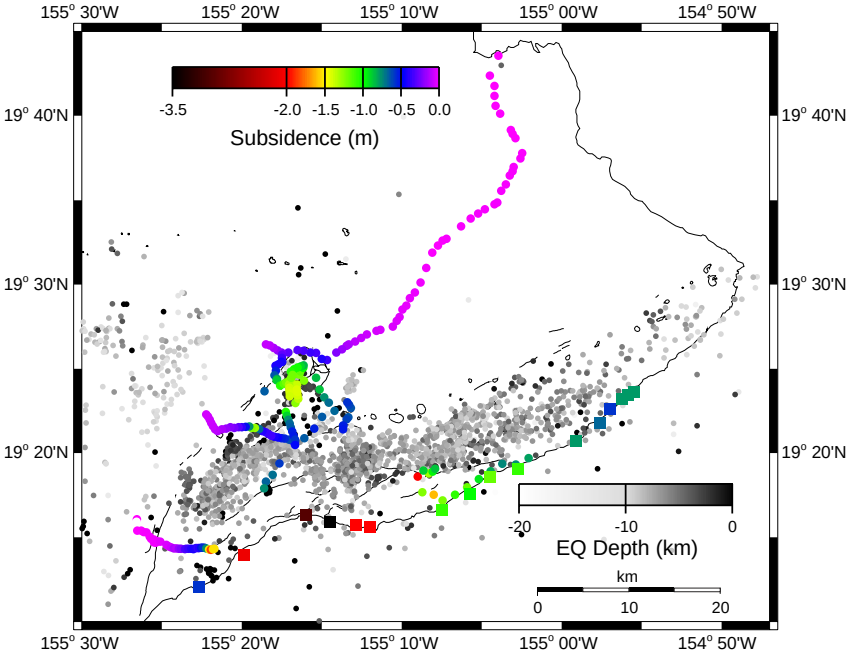

Fig. 5. Elevation changes relative to tide gage station at Hilo from repeated leveling measurements spanning the Kalapana earthquake (Lipman et al., 1985). Subsidence magnitude is indicated by color scale. Note the localized subsidence of the summit caldera and over the southwest rift, a lack of localized deformation across the upper east rift, southward tilt of the upper south flank, and localized northward tilting of individual blocks in the hanging wall of the Poliokeawe, Apua, and western Hilina Palis. Elevation changes shown across western Hilina Pali assume zero-elevation change of the northwestern-most site. Also shown are coastal elevation changes from tide gages and sea level changes (Lipman et al., 1985). We exclude the level lines across the Hilina faults (Great Crack and Chain of Craters Road lines) and the coastal subsidence data in our model inversions (Figs. 8–10).

west and to a lesser extent along the east rift zones. The caldera subsidence, centered near its southern rim, is close to previous estimates of the location of the underlying active magma reservoir (Dvorak and Dzurisin, 1993; Yang et al., 1992). The subsidence to the southwest of Kilauea caldera appears to lie about 2 km south of the mapped surface trace of the southwest rift zone. However, subsidence is coincident with shallow seismicity alongside the rift and subsidence during the 1974 southwest rift intrusion, indicating that the active rift zone is offset from the surface trace.

Subsidence along the coast measured by leveling exceeds 1 m near Kaena Point (Fig. 2). Also shown (as squares in Fig. 5) are the coastal subsidence measurements derived from relative sea-level changes (Lipman et al., 1985), with a downward displacement of ~3.5 m observed near Halape. Overall, the subsidence is greatest south of the segments of the Hilina fault system that slipped during the event. Localized downward displacement and northward tilting can be observed in the hanging wall of the Hilina faults that slipped during the event (south of the Apua and Poliokeawe Palis near $-155^{\circ}08'$ longitude and south of the Hilina Pali near $-155^{\circ}22'$ longitude. See Fig. 2). When modeling the data for slip on the coseismic rupture, we exclude elevation changes and trilateration data of sites clearly affected by Hilina Pali slip, as we do not attempt to include shallow failure on the Hilina Pali in our models.

3.2. Ground-surface tilt

The Uwekahuna tilt record shows that the summit was inflating during the several years preceding the earthquake (Fig. 4). Rapid deflation in December 1974 was caused by an intrusion and associated seismic swarm along the southwest rift zone; as part of the same event, an eruption occurred along the upper rift zone. Following the 1974 event, summit inflation resumed and continued until the Kalapana earthquake.

Tilt measurements around the caldera were conducted several times yearly using water-tube and spirit level methods (Okamura, 1988). Okamura (1988) describe the measurement techniques and their precision, list the observation history of each tilt network, and tabulate all the acquired data. Fig. 6 shows the observed tilt that accumulated between September 1975 and December 1975/January 1976. The tilt measurements are dominated by tilt towards the summit caldera, caused by the deflation of the summit magma reservoir during and immediately following the earthquake. Two sites located south of the Koae fault zone and north of the Hilina fault system (Hilina Pali and Kipuka Nene) show SSE-ward tilts of the upper south flank of about 100 μrad.

3.3. Trilateration measurements of horizontal deformation

Level and tilt measurements are concentrated near Kilauea caldera, and are therefore most affected by the magma redistribution during the Kalapana events. Trilateration measurements spanning most all of Kilauea provide valuable information about the coseismic rupture at depth. The entire network was surveyed in the fall of 1974 (Fig. 4) and the summit was surveyed almost monthly in 1975 (Lipman et al., 1985). Only a small subset of the network was occupied between the large 31 December 1974 intrusion in the southwest rift and the Kalapana earthquake. Our eventual data set includes 230 range changes of line lengths collected during 1974.73–1974.93 and 1975.92–1976.40 (Fig. 4).

A time series of extension of a trilateration line across Kilauea caldera (HVO113-HVO114) shows that Kilauea caldera swelled in 1975, was "stretched" even farther in the earthquake, contracted immediately following the coseismic rupture, to resume extending again during much of 1976. Thus, some of the data are strongly affected by deformation not related to the coseismic rupture, in particular the deformation from the 1974 rift intrusion (Fig. 7), summit magma chamber fluctuations, and postseismic deformation. We consider the summit chamber deformation and postseismic deformation independently, but correct the data for the effects of the 1974 south west rift intrusion as described below.

Because the western south flank measurements are significantly affected by the 31 December 1974, southwest rift intrusion, we correct the changes in baselines length by subtracting the contribution from this event (Fig. 7). Using trilateration data spanning the intrusion, collected in October of 1974 and January 1975, we used a non-linear optimization algorithm to find the best-fitting elastic dislocation model

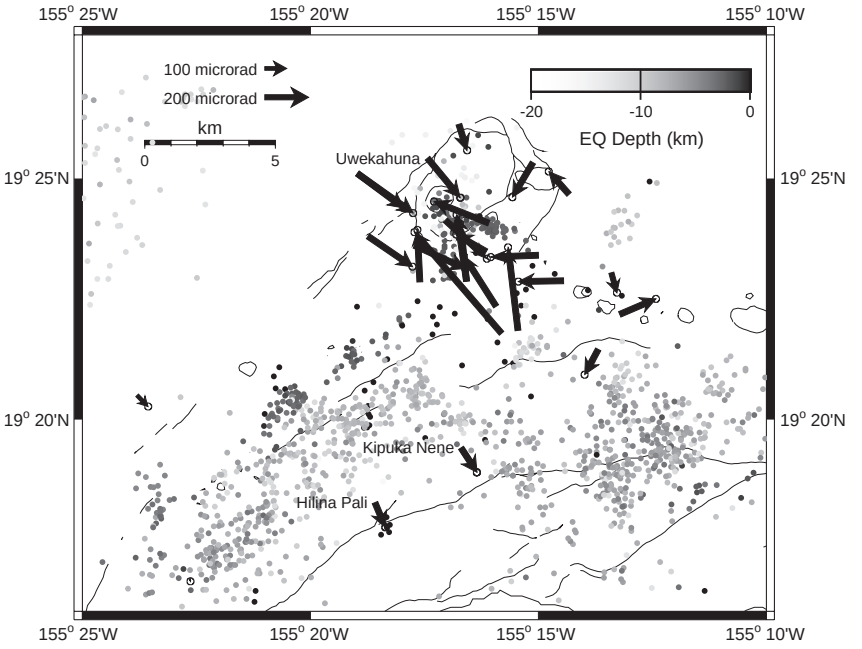

Fig. 6. Tilt associated with the 1975 Kalapana earthquake from water-tube and spirit-level measurements (Okamura, 1988). The data are dominated by tilt towards the southern end of Kilauea's caldera, the purported location of the summit magma chamber. Tilts near the southwest and east rift zones divert from this simple pattern, indicating tilt towards and away from the rifts, respectively. Two tiltmeters on the upper south flank at Hilina and Kipuka Nene show tilt to the southeast. Microseismicity (color-coded by depth) shown occurred during the time spanned by the tilt observations (September 1975 through December 1975/January 1976).

(e.g. Owen et al., 2000). The best-fitting model included a planar dike representing the intrusion and a collapsing sill representing the summit deflation (Owen and Bürgmann, 1999). The trilateration data spanning the earthquake were corrected by subtracting the line length changes predicted by the intrusion model to obtain the coseismic line length changes.

The horizontal displacements computed from the line-length changes we use in our model analysis are shown in Fig. 3. The site motions and their associated errors are computed using a model coordinate solution (Segall and Mathews, 1988) that minimizes translations and rotations of the network relative to model displacements of a detachment slip model. The horizontal displacement field is dominated by seaward motions of up to 8 m, increasing towards the coast, and by steep displacement gradients to the west and smaller strains to the east. Displacements decay to less than a meter well east of the southwest rift zone near the coast, suggesting that it did not bound the western extent of the rupture. The few stations located north of the rift zones show insignificant motions. Note that the sites with the largest displacements are located south of the Hilina fault system, which experienced up to 2 m of slip in the event (Lipman et al., 1985; Cannon et al., 2001). As these sites have apparently been strongly affected by shallow rotational slumping of the Hilina fault blocks (Cannon et al., 2001), we exclude the displacements shown as open arrows in Fig. 3 in our model inversions for slip on the deep detachment rupture.

4. Model inversions and deformation sources

Our approach to modeling the deformation of the 1975 Kalapana earthquake is to use elastic dislocations and constrained non-linear inversion to find the geometry of best fitting sources of deformation. Accordingly, deformations are characterized by slip or opening across rectangular surfaces buried in a homogenous, isotropic and elastic half-space

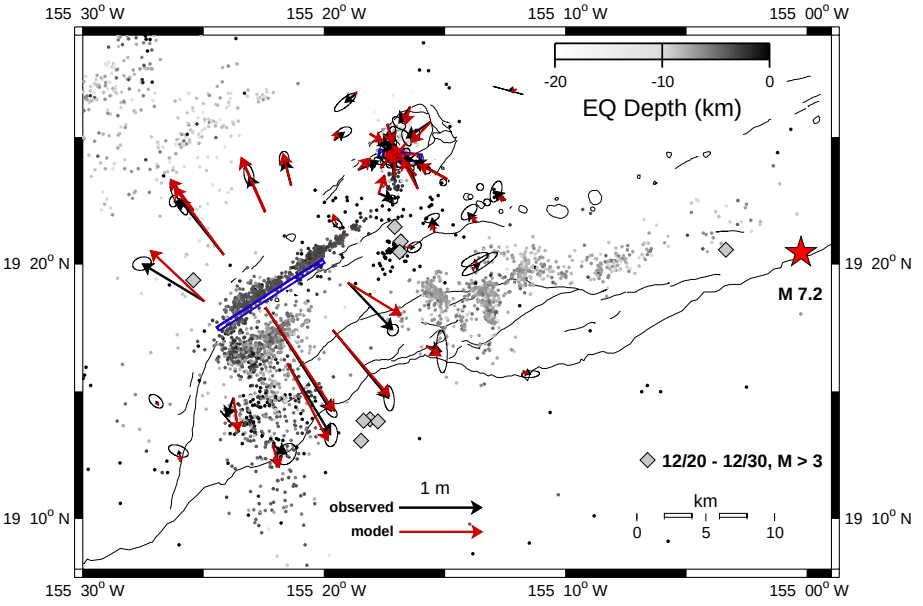

Fig. 7. Deformation associated with the 31 December 1974 southwest rift intrusion and predicted displacements from a distributed-opening model (Owen and Bürgmann, 1999). Observed (solid arrows with 95% confidence ellipses) and modeled (open arrows) horizontal displacements determined by trilateration and observed (gray shaded arrows with 95% confidence ellipses) and modeled (open gray arrows) tilts. The surface projections of the deformation sources are shown as bold gray-shaded outlines. Line length changes predicted by this model are removed from the trilateration measurements that span both events. The shallow microseismicity during the month following the rift intrusion closely matches the location of the model rift. Note the large cluster of induced seismicity reaching well south of the rift zone. Also shown are the foreshocks of the 1975 Kalapana earthquake that occurred in the two h before the main event (star).

(Okada, 1985). We simultaneously estimate the geometry (parameterized by length, depth, width, dip, strike, location) and amounts of strike-slip, dip-slip, and opening of one or more faults that best fit the tilt, level, and trilateration data weighted by their formal uncertainties (Arnadottir and Segall, 1994; Bürgmann et al., 1997). Specifically, we seek models that minimize the weighted residual sum of squares, $\mathrm{WRSS}=(d_{\mathrm{obs}}-d_{\mathrm{mod}})^{\mathrm{T}}\mathrm{cov}^{-1}(d_{\mathrm{obs}}-d_{\mathrm{mod}})$ where d_{obs} and d_{mod} are the observed and modeled deformation, respectively, and cov is the data covariance matrix. In some cases we apply bounds to some parameters (such as constraints on the depth of faulting or range of permissible fault strikes) to find best-fitting sources that are additionally constrained by geologic or seismic information. We model relative elevation changes between each benchmark pair scaled by the variances, which increase with the square root of distance along the leveling line (as 0.22 $\mathrm{mm}\sqrt{\mathrm{km}}$). The correlations between neighboring level sections are accounted for (Arnadottir and Segall, 1994). We assume no correlation between the N–S and E–W components of tilt or the individual line length changes in the trilateration data.

For the model inversions, we use 150 leveling observations, measurements from 26 tiltmeters, and 200 EDM line length data, giving us a total of 402 data parameters. For most of the data, we used the formal errors for the observations in the data covariance matrix, and did not introduce any relative weighting between the data sets. In a region of very localized subsidence in the southwest rift zone, we increased the leveling data errors at 4 sites by a factor of 10 so that they would not influence the model.

The best-fitting model was found using a random cost search algorithm (Berg, 1993). This algorithm introduces an element of randomness in such a way as to maximize the likelihood of finding the true global minimum, and not a local minimum. In addition, the random cost algorithm is run several hundred times from randomly selected starting models, ensuring that the parameter space is adequately covered.

This method has been used to successfully find the best-fitting model from surface deformation data in several tectonic and magmatic studies (Murray et al., 1996; Owen et al., 2000).

4.1. Summit reservoir deformation

Models previously used to represent pressure changes within the Kilauea magma reservoir include simple Mogi spherical point sources of dilatation (Delaney et al., 1993; Dvorak and Dzurisin, 1993; Mogi, 1958; Yang et al., 1992), ellipsoidal point sources (Davis, 1986), finite spherical (Delaney and McTigue, 1994) and ellipsoidal chamber sources (Yang et al., 1988), and vertical (dike) or horizontal (sill) rectangular dislocation sources (Delaney and McTigue, 1994; Ryan et al., 1983). Initial model inversions used a Mogi spherical point source, but we found that use of a collapsing sub-horizontal sill, characterized by a horizontal dislocation element with negative opening, gave a better fit to the data. This is consistent with other volcanic studies have found that a sill fits the surface deformation better when the magma chamber is shallow (3–4 km deep) and there is dense surface deformation data (e.g. Amelung et al., 2000).

4.2. Deformation associated with the Kalapana earthquake

The horizontal displacements computed from the trilateration, leveling, and tilt observations provide abundant constraints for the deformation events associated with the Kalapana earthquake. We begin with the simplest possible earthquake source, a uniform slip detachment surface, as proposed by Ando (1979) and find the predicted displacements give an adequate representation of some general patterns of what was observed (Fig. 8). Yet, substantial residuals remain. In particular, displacements along the western and eastern south flank are strongly underpredicted and level and tilt observations are also not well matched, in particular near the summit region.

We therefore consider additional sources of deformation that apparently played a role in the deformation sequence. To develop an adequate model of the event, we require substantial rifting along the southwest rift zone, deflation of the magma reservoir beneath the summit caldera, and some rifting along the east rift zone. Slip along the Hilina fault system is also apparent in the data, but is not included in the elastic model due to the apparent complexity of the three-dimensional geometry of the faults. Instead, as previously discussed, we exclude data clearly affected by shallow Hilina faulting.

Fig. 9 shows the model with these added complexities; this model decreases the leveling residuals significantly, and overall provides a 71% reduction in the total data misfit. We determined this model by solving for the geometry and displacement discontinuity on four dislocations. The first three dislocations are permitted opening displacements only, and their a priori locations are roughly placed near the east rift zone, southwest rift zone and summit caldera. We furthermore constrained the dip angle for the rift zone to be 90° (vertical) since we do not have the surface measurement density near the rift zones to adequately constrain the dip of the rift zone. In studies of more recent south flank deformation that had greater data coverage around the rift zones, the observations have also been consistent with vertical, or near vertical rift zones (Owen et al., 2000). Because of the small subsidence values on the north flank, model inversions favor an unrealistically shallow fault plane. As a result, we require that the detachment fault be located at 8 km or greater depth so that the model result would be consistent with the fault plane depth as estimated by the seismic data. While it is possible that there was slip on shallower fault planes or internal deformation within the south flank triggered by the earthquake, we are primarily concerned with the fault slip along the rupture plane for the Kalapana earthquake. No other constraints are imposed in the non-linear inversion. The model parameters for the best-fit model are given in Table 1. It should be noted that this model is not unique and there are uncertainties associated with these model parameter values. We do not attempt to quantify extensively the model parameter uncertainties, but will note that the summit model parameters are the best determined of the values. The quantification of our dislocation model errors would not be that enlightening since these uncertainties would not account for unquantified errors in the coseismic data (i.e., postseismic deformation that is impossible to independently quantify and remove) and the unquantified errors associated with our modeling assumption

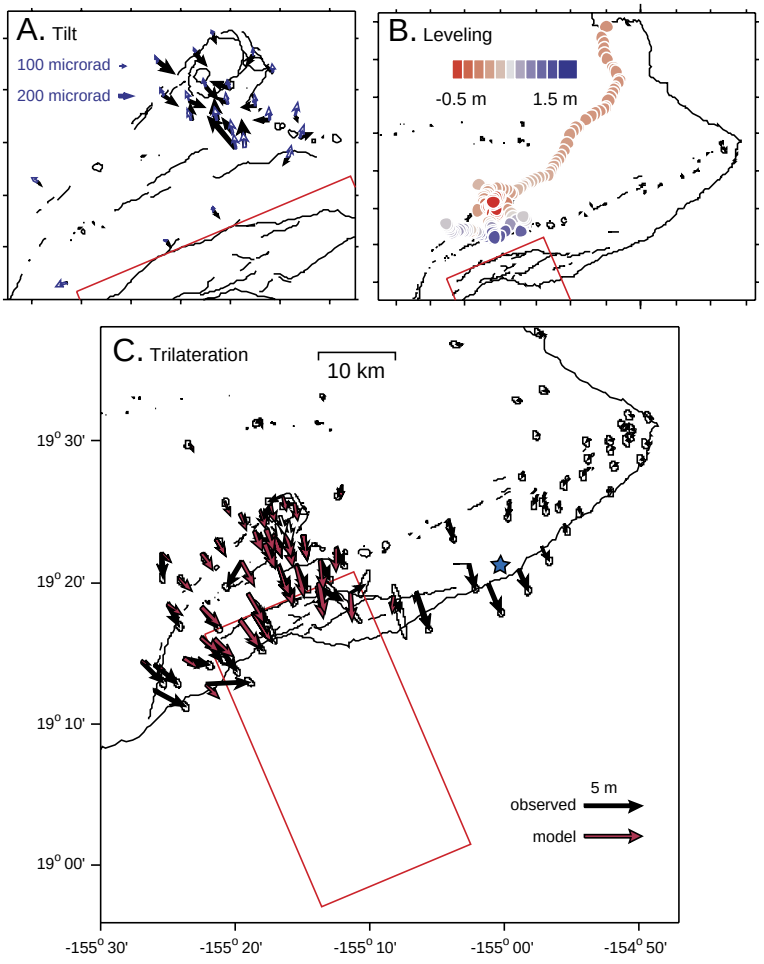

Fig. 8. Single fault dislocation model of Kalapana earthquake computed from non-linear inversion of trilateration, tilt, and leveling data. We exclude data that is affected by shallow deformation of the south flank due to Hilina fault slip (Figs. 5 and 6). (A) Tilt observations (solid black vectors) and model-predicted values (open blue vectors), (B) vertical displacement from leveling (plotted as residuals), and (C) trilateration data, excluding data affected by shallow deformation due to Hilina fault slip. The red lines indicate the surface projection of the fault plane. The 1975 M7.2 earthquake epicenter is shown with a blue star. (For interpretation of the references to colour in this figure legend, the reader is referred to the web version of this article.)

of using dislocations in a homogeneous elastic half-space.

Once the geometry of all four sources was determined, we further discretized the detachment fault into smaller dislocation planes, to allow for some slip heterogeneity on the irregularly shaped rupture. This fault plane area was increased, since the uniform slip model could be a conservatively small estimate of fault plane area that slipped in the earthquake. In order to represent our decreasing ability to constrain slip estimates with distance from the coast, the size of the discretized patches increases with distance offshore (Fig. 10). For the distributed slip model, we follow the methodology outlined in Harris and Segall (1987) and in Owen et al. (2000). In this case, however, the inversion is not a completely underdetermined problem since we have 402 data parameters from the leveling, tilt, and EDM measurements, and a total of 77 model parameters. We still use a singular value decomposition to calculate the weighted least squares estimate of the inversion. We use a finite difference approximation of the Laplacian to impose smoothness

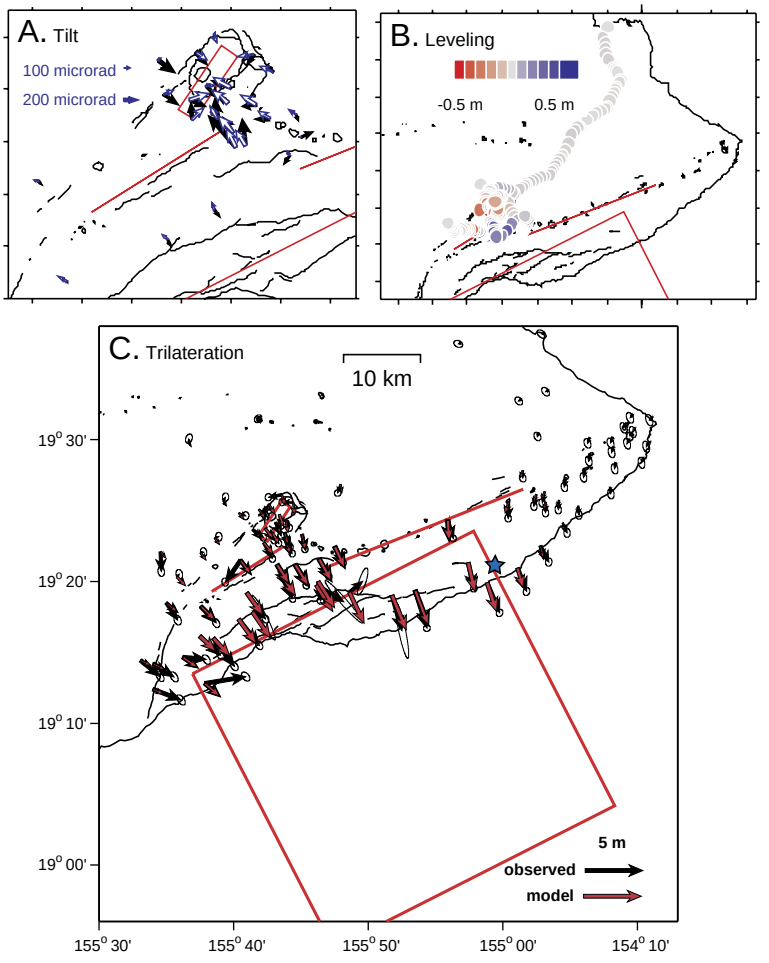

Fig. 9. Fault, rift zone, and summit sill model of Kalapana earthquake computed from non-linear inversion. The model was constructed from (A) tilt (solid black vectors are the observations, and open blue vectors are the model-predicted tilt values), (B) vertical displacement from leveling (plotted as residuals), and (C) trilateration data, excluding data affected by shallow deformation due to Hilina fault slip. The red lines indicate the surface projection of the dislocations used in this model. See Table 1 for details on the geometry and magnitude of these dislocations. The 1975 M7.2 earthquake epicenter is shown with a blue star. (For interpretation of the references to colour in this figure legend, the reader is referred to the web version of this article.)

constraints on the final slip distribution for the portion of the decollement beneath the subaerial edifice (Harris and Segall, 1987; Menke, 1989). We also use a bounded value least squares algorithm (Stark and Parker, 1995) to put positivity constraints on all of the fault slip and rift opening estimates. No constraint was put on the summit sill collapse value, which was estimated simultaneously with the rift opening and fault slip. The fault slip values for the fault patches were required to be between 0 and 12 m (where positive slip is defined as seaward-directed dip-slip). If no upper bounds are put on the fault slip, the estimated fault slip values can be as high as 30 m, but in a small, concentrated region just offshore of the south flank. By applying an upper bound of 12 m, we do not increase the data misfit significantly and we obtain a more realistic pattern of fault slip. The rift zone opening was constrained to be between 0 and 5 m. This maximum allowable rift opening value was chosen to keep the misfit to the north flank leveling data minimal. It is possible that some sections of the rift zone decreased in volume during the eruption, for

Table 1
Parameter estimates for uniform slip model. Length is dislocation length along strike, width is dislocation length perpendicular to strike (down-dip), depth is defined as the distance to the middle point of the lower dislocation edge, and the positions are the coordinates for middle point of the lower dislocation edge

Source	Len (km)	Wid (km)	Depth (km)	Dip	Strike	Slip/opening (m)	Latitude	Longitude
Fault	41	41	8.4	3	65	7.1	19.309	−155.210
Summit sill	5.4	1.4	3.7	17.2	33.4	−5.2	19.401	−155.277
SW rift	11	4	6.2	90[a]	58	3.3	19.348	−155.316
East rift	28	4.2	7.6	90[a]	68	5.3	19.396	−155.098

[a] Parameter values were fixed to those values in the model inversion.

instance if magma stored within the rift zone migrated from one area to another within the rift zone. However, in regions where we have strong control on the rift zone deformation, the data is consistent with pure extension across the rift zone. Inversions that allowed collapse along the rift zone only showed negative rift opening in regions where there were relatively poor constraints on the model.

The deformation data did not put strong constraints on the offshore fault slip values, and the initial distributed slip inversions tended to have the largest slip values on the fault patches that were furthest off shore (and therefore least constrained by the data). These models also had total geodetic moment values that were significantly larger than the Ma et al. (1999) and Nettles and Ekstrom (2004) estimates. Therefore we required that the distributed slip inversion produce an offshore uplift volume of 1.92 km^3, the uplift volume produced by the dislocation model used by Ma et al. (1999). This is not as large as the estimated 2.5 km^3 volume of water displaced to produce the tsunami, but we are not including in our model deformation related to the Hilina Pali faults, which probably caused significant uplift offshore.

4.3. Estimated sources of deformation

4.3.1. Caldera collapse

Subsidence of up to 1.5 m near the caldera during the 1975 earthquake suggests rapid draining of the shallow magma reservoir, presumably due to magma motion into the opening rift zones immediately following the event (Delaney et al., 1993; Dzurisin et al., 1980; Klein et al., 1987). Our non-linear inversion for the size and depth of the caldera source element finds it to lie in the same region as inversion studies of previous caldera events (Delaney and McTigue, 1994; Dvorak and Dzurisin, 1993; Yang et al., 1992). In the uniform slip model, the element is located at 3.7 km depth and has a negative opening of 5.2 m, suggesting removal of about 0.04 km^3. This compares with previous estimates of 0.04–0.09 km^3 (Dzurisin et al., 1980). The distributed slip inversion gives a negative opening value of 5.6 m, giving essentially the same volume loss.

4.3.2. Rift opening

Rift opening associated with the Kalapana earthquake is evident in localized subsidence of up to 1 m across the upper southwest rift zone (Fig. 5). Subsidence occurred in the same location as during previous rift intrusions, which are also well located by their associated shallow seismicity (Klein et al., 1987). It is also evident in the low values of subsidence measured on the north flank. A thrust-faulting earthquake of the size of the Kalapana earthquake should produce significant broad regional subsidence along the section of the leveling line that runs from Hilo to the volcano summit. The absence of this broad subsidence signature can be explained by opening within the deep rift zone, which would cause uplift that cancels out the earthquake-related subsidence.

Unfortunately, the trilateration data does not put much constraint on the opening magnitude and the length and depth of the opening rift segment. The opening was inferred to be in the mid-to-deep section of the southwest and east rift zone. Opening along 28 km of the east rift zone provided the best fit the geodetic data. We found that only a short section of the southwest rift zone experienced opening of 3.3 m, even though there was significant deformation observed in the trilateration data in the lower southwest rift zone. This section of the southwest rift zone corresponds to the same region as that of the 1974

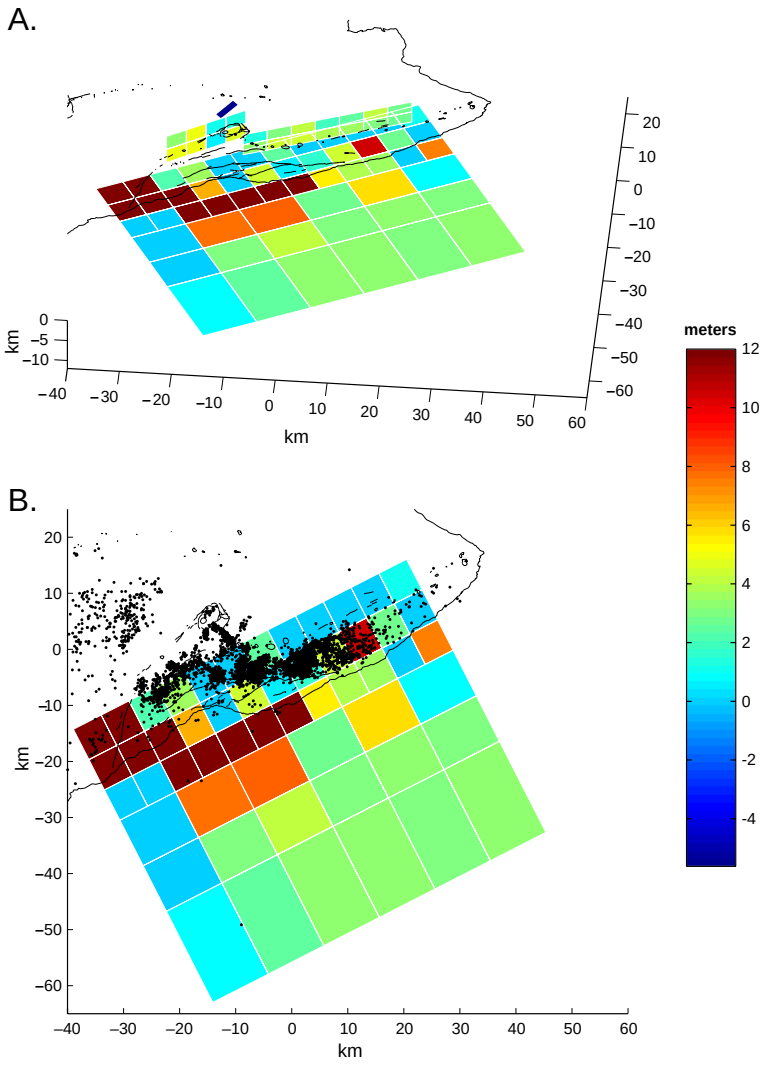

Fig. 10. Slip and opening distribution inferred from tilt, leveling and trilateration data. (A) View of deflation of summit sill, opening of rift zones, and dip-slip along the detachment (B) View of dip-slip along the detachment and aftershocks from the Kalapana earthquake. Shown are the epicenters from immediately following the mainshock until September 1977. Note that the majority of the aftershocks on the south flank occur in regions of low fault slip, except for around the actual initiation point of the rupture.

intrusion. Although we removed estimated displacements associated with this intrusion, there may have been significant post-intrusion and pre-earthquake extension in that region.

The pattern of rift opening in the distributed slip model is relatively smooth along the east rift zone, with the opening being larger along the deeper segments of the model. Within the southwest rift zone, the distributed opening model shows a more localized region of extension. This result is strongly constrained by the high density of leveling and tilt data in this region, although the model is complex in this region, with closely spaced dislocations from different elements of the magmatic system.

The total estimated volume of opening within the rift zone was 0.8 km^3 in the uniform slip model and 0.9 km^3 in the distributed slip model. This volume is an order of magnitude greater than the summit volume

collapse. The discrepancy in these volume estimates may be related to differences between the volume change estimated by simple elastic models, and the actual magma volume. Considerations like the pressure dependence of the magma volume may be important in order to accurately compare the summit volume collapse with the amount of opening in the rift zone. In addition, some of the rift zone opening may be due to mismodeling of extension that actually occurs on buried normal faults.

4.3.3. Detachment slip

The observed EDM displacements of 5 m or more are consistent with large displacement along a detachment fault at the base of the volcano. The fault plane that best fits the geodetic data, assuming uniform slip, is a 41-km-wide, sub-horizontal square with its northeastern corner roughly located at the rupture initiation point. The estimated depth is 8.4 km. The estimated slip is 7.1 m, which results in a geodetic moment of 3.6×10^{20} Nm assuming a rigidity of 30 GPa. When we allow spatial variation in the slip along the detachment, some new features in the fault slip pattern appear. There are local maxima in the fault slip south of the rupture initiation point, along the coast in the central section of the south flank, and also along the lower southwest rift zone. The high slip in the lower southwest rift zone is a persistent feature of the inversions, even when we constrain the edges of the detachment to have low slip values. However, there is likely some deformation in the lower southwest rift zone that was not related to the Kalapana earthquake. There was significant seismicity in this region (Fig. 7) in response to the 31 December 1974 rift intrusion and so there is some ambiguity as to whether or not the slip in the southwest rift zone is related to the Kalapana earthquake or the 1974 rift intrusion. The total geodetic moment for the distributed slip model is 4.1×10^{20} Nm. The pattern of slip shows the highest fault slip values in regions where there are few aftershocks.

5. Discussion

We find that a combination of near-surface shallow slumping, volcanic deformation sources and slip on the detachment fault near the base of Kilauea's edifice is required to explain the observed surface displacements from the Kalapana earthquake. Despite the significant number of model parameters we significantly misfit the data, as is expressed in a 75% reduction of variance, which leaves 25% of the signal unexplained by the model sources of deformation (see Fig. 9 and Fig. 11 for model misfit). As the complex shallow deformation due to slip on the Hilina faults is not appropriately modeled with elastic dislocations, we removed the geodetic surveys in the hanging wall of the Hilinas from the model inversion. We follow Delaney et al. (1993) in arguing that the remaining misfit is unlikely to be due only to overly optimistic data error estimates. Rather, the remaining misfits are likely a reflection of the complexity of Kilauea deformation, as well as being due to significant contrast in the material properties of the south flank, the rift system and the old oceanic crust (Du et al., 1994). While we believe that our models reveal much of the processes taking place during and immediately following the 1975 Kalapana earthquake, we realize that the south flank of Kilauea Volcano is not an ideal elastic half-space. Our model does not include fault systems like the Koae normal fault system near the summit, nor does it allow for internal deformation of the edifice, which we discuss qualitatively below (Section 5.3).

5.1. Relationship of deformation with microseismicity

The aftershocks of the 1975 earthquake are restricted to a 5-10-km-wide zone bordered by the Kilauea rift zones to the north and west, and by the surface trace of the Hilina fault zone to the south (Figs. 6 and 10b) (Klein et al., 1987; Lipman et al., 1985). This corresponds to the approximate width of the high-density dike complex at the base of the volcanic edifice (Hill and Zucca, 1987). Little microseismicity occurs south of the Hilina fault zone, despite the large amount of coseismic slip that occurred there (Fig. 10b). It is likely that the distribution of microseismicity is not a direct reflection of the occurrence or magnitude of aseismic slip but differs depending on the frictional properties of the fault zone.

Gillard et al. (1996) analyzed 870 focal mechanisms occurring between 1972 and 1992 at depths <20 km on Kilauea's south flank. As focal mechanisms

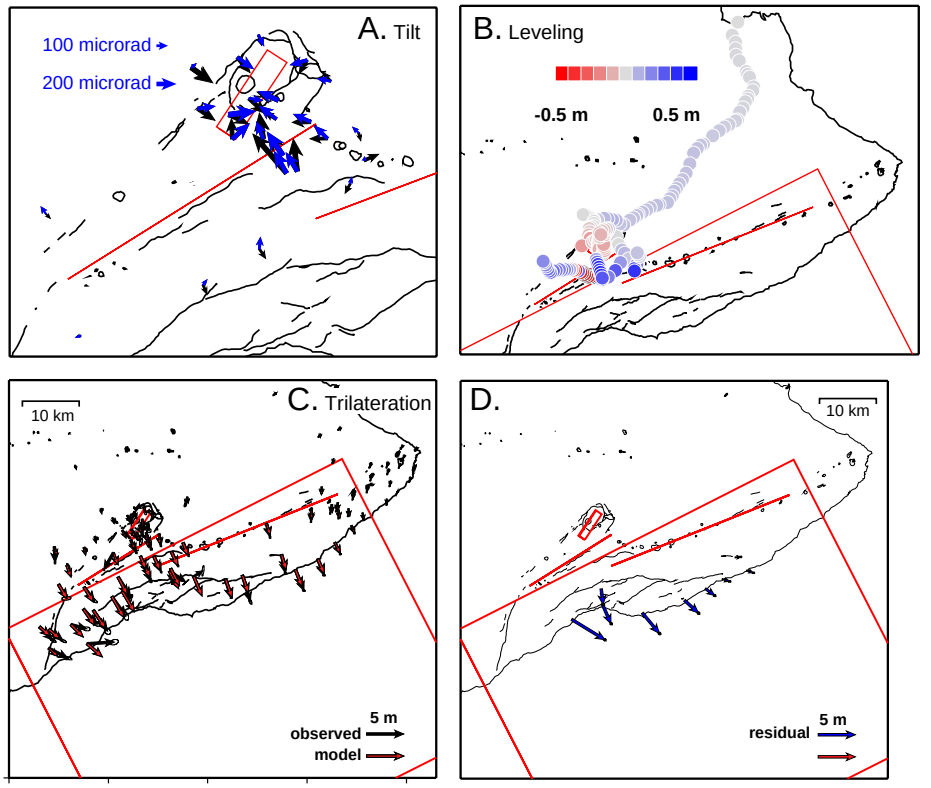

Fig. 11. Comparison of observed and model-predicted deformation from model shown in Fig. 10. (A) Tilt data vectors, with observed in solid black and model-predicted in blue outline, (B) leveling residuals, and (C) trilateration data show that this model fits the major patterns of the coseismic geodetic data, but that there are still some significant residuals. These residuals are most likely due to the complexity of the deformation on the south flank not included in our model. (D) Residuals between model-predicted displacements and the trilateration data on the hanging wall of the Hilina fault system. These data were not used in the inversion, and show that several meters of displacement at these coastal sites are not explained by slip along the detachment, even when the total geodetic moment is equivalent to a M_w7.7 earthquake. These residuals are consistent with shallow slumping along the Hilina Pali fault system, as discussed in more detail by Cannon et al. (2001). (For interpretation of the references to colour in this figure legend, the reader is referred to the web version of this article.)

give some indication on the state of stress in the crust, we can compare the seismic results with our 1975 earthquake model. Detachment events represent about 50% of all events in the 20-yr period, there have been no strike-slip events at all. In the 3 yr prior to the Kalapana earthquake no normal faulting events occurred east of latitude −155 °10'W. Normal faulting on NE striking faults occurred in the year prior to the event in a broad zone SE of the SW rift zone, possibly related to detachment slip associated with the 31 December 1974, southwest rift intrusion. Otherwise the pre-earthquake south flank seismicity was characterized by reverse and detachment focal mechanisms at 6–11 km depth. In particular, reverse faulting events occurred at a maximum rate in the 3 pre-Kalapana years suggesting that the south flank was under compression in that time period across much of its width.

Following the 1975 earthquake normal faulting initiated north of the Hilina faults, suggesting tension in that region. This agrees with our conclusion that slip occurred predominantly south of the Hilinas. In agreement with a tensile postseismic stress regime are the 24 east rift intrusions that occurred since the event (1975–1986) (Klein et al., 1987). Detachment events occurred at a high rate since the event and increased in the eastern south flank around 1985. These events accompany continued south flank seaward motion since the event (Delaney et al., 1993; Owen et al., 1995).

5.2. Segmentation of south flank deformation

Lateral, strike-slip dominated boundaries of the mobile south flank block are not well defined. Bathymetric data suggest an offshore lineament coincident with the western boundary of the mobile zone. Morgan et al., 2003, present evidence for ~3 km of right lateral displacement along this lineament in the vicinity of Papa'u seamount, however, no obvious signs of right-lateral shear have been observed on land (R. Fiske personal communication, 1994). The offshore ridge appears to be linked to the western termination of large Hilina scarp heights as well. Denlinger and Okubo (1995) suggest that shear is taken up through oblique opening along the southwest rift zone of Kilauea. However, both the 1975 coseismic motions, as well as the south flank motions currently measured by GPS (Owen et al., 2000) diminish well to the east of this boundary. Therefore, very large shear strains must have accumulated in this region in the last 20 yr. This small portion of the active south flank may represent a potential future M~6 earthquake source. Alternatively, the southwest rift zone is itself mobilized by detachment faulting of Mauna Loa's south flank in 1868-type earthquakes (Wyss, 1988). This region also releases strain in M~6 earthquakes, as shown recently by the 1999 M5.9 earthquake on the detachment fault underneath Mauna Loa and the southwest rift zone. While the edge of the detachment fault in the uniform slip model of the 1975 event ended well to the east of the southwest rift zone, the distributed slip model showed up to 12 m of slip in this region. Due to the nature of trilateration data, there are relatively weak constraints on the orientation and magnitude of the vectors in this region. The observed vectors change significantly depending on which model is used to estimate the displacements using a model-coordinate solution. However, given that very little displacement has been seen in this region since 1975 except for the 1999 M5.9 earthquake (Delaney et al., 1998; Owen et al., 2000), it is possible that this is a region of the detachment fault that ruptures in seismic events and does not experience the aseismic creep observed underneath the central south flank.

Northwest oriented lineations of low electrical resistivity on the eastern south flank (Flanigan and Long, 1987) may indicate left-lateral tear faults that bound the detached block to the east. These lineaments may be related to the segmentation of the detachment, but there is no well-expressed topographic signature of this deformation. Another northwest trending high conductivity zone near the eastern end of the east rift zone coincides with the eastern boundary of the 1989 aftershock zone, and may delineate the eastern extent of the south flank block. Offshore studies also see some evidence for an eastern boundary, with seismic reflection data showing contrasting structure of the submarine flank across this eastern boundary zone (Hills et al., 2002) and Morgan et al. (2003) finding evidence for an old landslide scar in this same region.

The 1989 earthquake rupture zone (Arnadottir et al., 1991) abuts the 1975 slip plane at its eastern edge. That is, the 1989 event extended the slipped portion of the detachment system to the east. Slip in the 1989 earthquake was much less than in 1975, suggesting that either the slip rate (and associated rift expansion rate) diminishes to the east, or that less of a slip deficit remained from the 1868 earthquake that ruptured much of the south flank detachment system bounded by Mauna Loa's and Kilauea's rift zones (Wyss, 1988; Wyss and Koyanagi, 1992b). The aftershock regions appear to correlate mostly to regions north of the maximum slip in the two events. Little seismicity before or after the earthquakes is observed over much of the detachment surface south of the Hilina faults.

The 1975, 1989, and several smaller earthquakes have all nucleated from the same region of the south flank, although they don't necessarily propagate in the same direction. From an analysis of the south flank microseismicity, the Kalapana region has been identified as a region that experiences recurring periods of quiescence, which may be precursors to earthquakes or related to magmatic activity in the east rift zone (Dieterich and Okubo, 1996). This region has not shown up as strongly anomalous region in the more recent campaign GPS data (Owen et al., 2000), although it is on the eastern edge of the creeping zone. Continuous GPS data is currently being collected above this nucleation region and drastically increases our temporal resolution of deformation in this area.

5.3. Role of Hilina faulting in coseismic south flank deformation

Ground deformation and faulting in the 1975 earthquake was nearly continuous along a 25-km-long

zone of the Hilina Pali fault system. The largest normal offsets occurred along the northernmost scarps and no apparent fault slip can be recognized east of the epicenter. Total vertical offsets along the fault zone measured up to 2.5 m, about 60% of the total coastal subsidence. This suggests that the fault zone represented a rather significant component of the coseismic deformation and plays an important role in the internal deformation of Kilauea's south flank. We find that horizontal displacements of as much as 8 m and subsidence in excess of 3 m between Kaaha and Apua are difficult to explain unless detachment slip of as much as 35 m occurred in that region. Residuals at these coastal sites using the distributed slip model (Fig. 11d) show that even 12 m of slip along the detachment falls several meters short of predicting the full displacement vectors. The residual vectors show an increasing trend with distance from the fault scarp, which is consistent with shallow listric faulting. Back tilting of the hanging wall of two Hilina faults is evident in the leveling line up the Chain of Craters Road (Lipman et al., 1985). The amount of back tilting is compatible with a relatively shallow listric fault geometry that is decoupled from the primary rupture at depth (Cannon et al., 2001) (Fig. 1b).

5.4. Slip-distribution on the main rupture

The distribution of slip on the detachment fault shows most of the slip occurring closer to the coast and offshore region than do the focal mechanisms of subevents proposed by Harvey and Wyss (1986) from forward modeling of two strong motion records. We tested inversions that added a strike-slip component to see if we could resolve systematic variations in the rake, but the changes in the model estimate appeared somewhat randomly oriented.

5.5. Comparison with tsunami data

Observations of the timing and magnitude of the tsunami generated by the Kalapana earthquake provide additional constraints about the 1975 events. Models developed to explain the tsunami differ significantly (Ando, 1979; Ma et al., 1991, 1999), however, most studies suggest source areas in excess of 2000 km^2 with average displacements of about 1 m displacing a volume of ~2.5 km^3 (Ma et al., 1999). The large size of the tsunami compares favorably with the seismic moment suggested by Nettles and Ekstrom (2004) and also with aseismic shallow slumping during the event (Ma et al., 1999). The source investigation by Ma et al. (1999) suggests an origin of the tsunami near the toe of the Hilina slump, defined by the offshore bench shown in Fig. 2. The preferred model is a slump with 1 m of subsidence along the coast and 1 m of uplift offshore, but a wide dislocation model, similar to the one we present here, also satisfies the data (Ma et al., 1999). Ma et al. (1999) prefer the slump model because it is more compatible with the lack of aftershocks offshore and the coastal deformation. We can fit the volume of uplift estimated by the wide dislocation model of Ma et al. (1999) (1.92×10^3 km^3) and also provide a reasonable fit to the geodetic data using the distributed slip model. While the uplift volumes for these dislocation models are less than the inferred volume of water displaced (2.5×10^3 km^3), both our study and Ma et al. (1999) ignore shallow faulting along the Hilina Pali, which could provide some significant offshore uplift if we assume that these normal faults curve into a shallow detachment fault at 3–5 km depth (Cannon et al., 2001).

5.6. Post-earthquake vs. coseismic deformation

In the two decades since the Kalapana earthquake, the summit of Kilauea continued to subside adding another 2 m to the 1.5 m of coseismic lowering, accompanied by 2.5 m of post-earthquake extension across the summit (Delaney et al., 1998). Slight contraction of trilateration baselines across the south flank from 1976 to 1981 gave way to insignificant extensional strains from 1981 through 1995. Owen et al. (2000) find that 16-cm/yr basal shear and deep-rift opening can explain GPS (Global Positioning System) measurements from 1990 to 1996; this GPS study also shows slight extension across the south flank, opposite of the contraction seen prior to the 1975 Kalapana event. It is not clear if this mostly aseismic fault slip is due to postseismic adjustments or if aseismic creep on parts of the detachment system occurs continuously between seismic events. The aseismically slipping surface, not very well defined, apparently reaches from the rift zones to at least 20 km from the rift zones, as measured perpendicular to the strike of the

east rift (Owen et al., 2000). The lateral extent of rapid ongoing surface displacements and the 1975 deformation are about the same, suggesting significant overlap of fault slip 20 yr after the event with the coseismic rupture. Whereas crustal deformation data collected since 1975 indicates concurrent rift opening and aseismic basal fault slip (Delaney et al., 1990; Denlinger and Okubo, 1995; Owen et al., 1995) the rift zone was compressed by rift intrusions in the 80 yr before the 1975 earthquake (Swanson et al., 1976). There is little evidence of significant elastic strain accumulation since the Kalapana earthquake (Delaney et al., 1998) in marked contrast to the observations in the years leading up to the event.

5.7. The 1868 M7.9 Kau earthquake

The 2 April 1868 Kau earthquake was preceded by significant magmatic activity of Kilauea and Mauna Loa and 5 days of heavy foreshocks punctuated by a large event in southern Kau district (Hitchcock, 1912; Wood, 1914). Subsidence of 1.2 to 2.4 m along the southeast coast of Hawaii (Hitchcock, 1912) resembled that observed in 1975. In 1975 the maximum drop of 3.5 m occurred near Halape (Fig. 2). In 1868 the coastline segments that subsided more than 2 and 3 m were approximately 100 and 70 km long, respectively, with the maximum values near Apua (Wood, 1914; Wyss, 1988; Wyss and Gillard, 1992). Hitchcock (1912) reports extensive faulting (seaward settling) along the Hilina fault system. Eruptions were observed both along the southwest rift zone of Mauna Loa and Kilauea immediately following the earthquake (Hitchcock, 1912; Tilling et al., 1976). The Kilauea southwest rift apparently fractured along much of its length, widening and opening by more than 5 m and showing some evidence for strike-slip motion (Wood, 1914).

Observations of tsunami heights at destroyed villages along the coast and on the other Hawaiian islands (Wood, 1914) also suggest a rupture that was larger but similar in nature as the 1975 event. Wyss (1988) estimates the magnitude of the 1868 event to be about 7.9 ($M_o \geq 10^{21}$ Nm) and suggests a 50 by 80 km rupture plane centered 50 km SW of the 1975 epicenter. The above observations suggest that the 1868 rupture did break from the southwest rift of Mauna Loa across Kilauea's south flank and that slip increased east and south of Kilauea's southwest rift. Assuming a similar mechanism of subsidence and tsunami generation, we find that the magnitude of slip in the Kilauea portion of the rupture may have been comparable to those in 1975. If the 1975 earthquake released the accumulated strain on the basal detachment since the 1868 rupture, we may expect similarly sized ruptures on a ~100 yr cycle. The strain accumulation on the detachment fault, which is potentially due to the growth and extension of the rift zones, is likely less uniform and steady-state than along plate-bounding faults. However, the magma supply rate for Kilauea Volcano is remarkably uniform compared to other volcanoes around the globe. The lack of any observed significant strain accumulation on the south flank since the 1975 rupture would be consistent with the south flank still being at the early stages of a new earthquake cycle.

6. Conclusions

The geodetic observations from the 1975 Kalapana earthquake show a complex pattern of deformation. The large earthquake on the volcano's basal detachment triggered faulting along the Hilina Pali, extension within the rift zone, and a summit eruption and collapse of the summit magma chamber. The dense leveling and tilt data collected around the caldera put tight constraints on the summit deformation. We are able to fit the observations best with a collapsing sill at 3.7 km depth underneath the summit caldera, and estimate 0.04 km^3 of summit deflation associated with the earthquake. EDM data and leveling data collected on the south and north flank, respectively, allow us to image the slip along the basal detachment and opening within the rift zone. In order to attempt to remove the first order effects of shallow slumping along the Hilina Pali faults, we model only data collected north of this fault system. The leveling data requires both opening within the southwest rift zone at mid-range depths and deep extension within the east rift zone. We find that the amount of fault slip required on the basal detachment by the geodetic data is consistent with the larger moment estimates from tsunami observations and recent analysis of the long period seismograms. We also find that the majority of the fault slip

occurred to the south and west of the hypocenter, and south of the region of microseismicity.

Acknowledgement

Financial support provided by U.S. Geological Survey NEHRP grant 14534-HQ-98-GR-1024 to RB and a U.C. Berkeley Miller postdoctoral fellowship to SO. This paper would not have been possible without the many years of dedicated data gathering, analysis, and archiving of the Hawaiian Volcano Observatory crustal deformation group. Thanks to Dominique Gillard for providing earthquake locations and focal mechanisms; to Jack Lockwood for providing copies of his fieldnotes from his post-earthquake observations; and to Jim Kellogg and Bill Chadwick for sharing their Hilina offset data with us. We thank Eric Cannon, Roger Denlinger, Mike Lisowski, Asta Miklius, and Paul Segall for discussions and advice and Thora Arnadottir and Julie Morgan for very helpful reviews. Berkeley Seismolab Contribution #04-xy.

References

Amelung, F., Jonsson, S., Zebker, H., Segall, P., 2000. Widespread uplift and 'trapdoor' faulting on Galapagos volcanoes observed with radar interferometry. Nature 407, 993–996.

Ando, M., 1979. The Hawaii earthquake of November 29, 1975: low dip angle faulting due to forceful injection of magma. J. Geophys. Res. 84, 7616–7626.

Arnadottir, T., Segall, P., 1994. The 1989 Loma Prieta earthquake imaged from inversion of geodetic data. J. Geophys. Res. 99, 21835–21855.

Arnadottir, T., Segall, P., Delaney, P., 1991. A fault model for the 1989 Kilauea south flank earthquake from leveling and seismic data. Geophys. Res. Lett. 18, 2217–2220.

Berg, B.A., 1993. Locating global minima in optimization problems by a random-cost approach. Nature 361, 708–710.

Bryan, C.J., Johnson, C.E., 1991. Block tectonics of the island of Hawaii from a focal mechanism analysis of basal slip. Bull. Seismol. Soc. Am. 81, 491–507.

Bürgmann, R., Denlinger, R., 1995. The role of the Hilina fault system in the deformation of the mobile south flank of Kilauea Volcano, Hawaii. IUGG XXI General, p. 455.

Bürgmann, R., Segall, P., Lisowski, M., Svarc, J., 1997. Postseismic strain following the 1989 Loma Prieta earthquake from GPS and leveling measurements. J. Geophys. Res. 102, 4933–4955.

Cannon, E.C., Bürgmann, R., Owen, S.E., 2001. Shallow normal faulting and block rotation associated with the 1975 Kalapana earthquake, Kilauea Volcano, Hawaii. Bull. Seismol. Soc. Am. 91, 1553–1562.

Clague, D.A., Denlinger, R.P., 1994. The role of dunite cumulate in destabilizing the flanks of Hawaiian volcanoes. Bull. Volcanol. 56, 425–434.

Crosson, R.S., Endo, E.T., 1981. Focal mechanisms of earthquakes related to the 29 November l975 Kalapana, Hawaii, earthquakes: the effect of structure models. Bull. Seismol. Soc. Am. 71 (3), 713–729.

Crosson, R.S., Endo, E.T., 1982. Focal mechanisms and locations of earthquakes in the vicinity of the 1975 Kalapana earthquake aftershock zone 1970–1979: implications for tectonics of the south flank of Kilauea Volcano, Island of Hawaii. Tectonics 1, 495–542.

Davis, P.M., 1986. Surface deformation due to inflation of an arbitrarily oriented, triaxial ellipsoidal cavity in an elastic halfspace, with reference to Kilauea Volcano, Hawaii. J. Geophys. Res. 91 (B7), 7429–7438.

Delaney, P.T., McTigue, D.F., 1994. Volume of magma accumulation or withdrawal estimated from surface uplift or subsidence, with application to the 1960 collapse of Kilauea Volcano. Bull. Volcanol. 56, 417–424.

Delaney, P.T., Fiske, R.S., Miklius, A., Okamura, A.T., Sako, M.K., 1990. Deep magma body beneath the summit and rift zones of Kilauea Volcano, Hawaii. Science 247, 1311–1316.

Delaney, P.T., Wyss, M., Lipman, P.W., Okamura, A., 1992. Comment on "Precursors to the Kalapana M-7.2 earthquake" by Max Wyss, F.W. Klein, and Arch C. Johnston. J. Geophys. Res. 97 (B4), 4839–4841.

Delaney, P.T., Miklius, A., Arnadottir, T., Okamura, A.T., Sako, M.K., 1993. Motion of Kilauea Volcano during sustained eruption from the Puu Oo and Kupaianaha vents, 1983–1991. J. Geophys. Res. 98, 17801–17820.

Delaney, P.T., et al., 1998. Volcanic spreading at Kilauea, 1976–1996. J. Geophys. Res. 103, 18003–18023.

Denlinger, R.P., Okubo, P., 1995. Structure of the mobile south flank of Kilauea Volcano, Hawaii. J. Geophys. Res. 100 (24), 499–524.

Dieterich, J.H., 1988. Growth and persistence of Hawaiian volcanic rift zones. J. Geophys. Res. 93, 4258–4270.

Dieterich, J.H., Okubo, P., 1996. An unusual pattern of recurring seismic quiescence at Kalapana, Hawaii. Geophys. Res. Lett. 23, 447–450.

Du, Y., Segall, P., Gao, H., 1994. Dislocations in inhomogeneous media via a moduli-perturbation approach: general formulation and 2-D solutions. J. Geophys. Res. 99, 13767–13779.

Dvorak, J.J., 1986. Mechanical response of the south flank of Kilauea Volcano, Hawaii, to intrusive events along the rift systems. Tectonophysics 124, 193–209.

Dvorak, J.J., Dzurisin, D., 1993. Variations in magma supply rate at Kilauea Volcano, Hawaii. J. Geophys. Res. 98, 22255–22268.

Dzurisin, D., et al., 1980. Geophysical observations of Kilauea Volcano, Hawaii: 2. Constraints on the magma supply during November l975–September l977. J. Volcanol. Geotherm. Res. 7 (3/4), 241–269.

Eissler, H.K., Kanamori, H., 1987. A single-force model for the 1975 Kalapana, Hawaii earthquake. J. Geophys. Res. 92 (B6), 4827–4836.

Flanigan, V.J., Long, C.L., 1987. Aeromagnetic and near-surface electrical expression of the Kilauea and Mauna Loa volcanic rift systems. U. S. Geol. Surv. Prof. Pap. 1350, 935–946.

Furumoto, A.S., Kovach, R.L., 1979. The Kalapana earthquake of November 29, l975: an intraplate earthquake and its relation to geothermal processes. Phys. Earth Planet. Inter. (18), 197–208.

Gillard, D., Wyss, M., Okubo, P., 1996. Type of faulting and orientation of stress and strain as a function of space and time in Kilauea's south flank, Hawaii. J. Geophys. Res. 101 (B7), 16025–16042.

Harris, R., Segall, P., 1987. Detection of a locked zone at depth on the Parkfield, California segment of the San Andreas fault. J. Geophys. Res. 92, 7945–7962.

Harvey, D., Wyss, M., 1986. Comparisons of a complex rupture model with the precursor asperities of the 1975 Hawaii M_s=7.2 earthquake. Pure Appl. Geophys. 124 (4/5), 957–973.

Hill, D.P., Zucca, J.J., 1987. Geophysical constraints on the structure of Kilauea and Mauna Loa Volcanoes and some implications for seismomagmatic processes. U. S. Geol. Surv. Prof. Pap. 1350, 903–917.

Hills, D.J., Morgan, J.K., Moore, G.F., Leslie, S.C., 2002. Structural variability along the submarine south flank of Kilauea volcano, Hawaii, from a multichannel seismic reflection survey. Hawaiian volcanoes: deep underwater perspectives. Geophys. Monogr. 128, 105–124.

Hitchcock, C.H., 1912. The Hawaiian earthquakes of 1868. Bull. Seismol. Soc. Am. 2, 181–192.

Kellogg, J.N., Chadwick, W., 1987. Neotectonic study of the Hilina fault system, Kilauea, Hawaii. Geol. Soc. Am. Abstr. w. Prog. 19 (6), 394.

Klein, F.W., Koyanagi, R.Y., Nakata, J.S., Tanigawa, W.R., 1987. The seismicity of Kilauea's magma system. U. S. Geol. Surv. Prof. Pap. 1350, 1019–1185.

Lipman, P.W., Lockwood, J.P., Okamura, R.G., Swanson, D.A., Yamashita, K.M., 1985. Ground deformation associated with the 1975 magnitude-7.2 earthquake and resulting changes in activity of Kilauea Volcano, Hawaii. U.S. Geol. Surv. Prof. Pap. 1276, 1–45.

Lipman, P.W., Normark, W.R., Moore, J.G., Wilson, J.B., Gutmacher, C.E., 1988. The giant submarine Alika debris slide, Mauna Loa, Hawaii. J. Geophys. Res. 93 (B5), 4279–4299.

Ma, K.-F., Kanamori, H., Satake, K., 1991. The origin of the tsunami excited by the 1975 Kalapana, Hawaii, earthquake ([abs.]). Eos, Trans., Am. Geophys. Union Supp. 72 (44), 331.

Ma, K.-F., Kanamori, H., Satake, K., 1999. Mechanism of the 1975 Kalapana, Hawaii, earthquake inferred from tsunami data. J. Geophys. Res. 104 (B6), 13153–13167.

Menke, W., 1989. Geophysical Data Analysis: Discrete Inverse Theory. Academic Press, San Diego, p. 289.

Mogi, K., 1958. Relations between the eruptions of various volcanoes and the deformations of the ground surfaces around them. Bull. Earthq. Res. Inst. 36, 111–123.

Moore, J.G., Chadwick, W.W., 1995. Offshore geology of Mauna Loa and adjacent areas, Hawaii. AGU Geophys. Monogr. 92, 21–44.

Moore, J.G., Moore, G.W., 1984. Deposit from a giant wave on the island of Lanai, Hawaii. Science 226, 1312–1315.

Moore, J.G., Normark, W.R., Holcomb, R.T., 1994. Giant Hawaiian underwater landslides. Science 264, 46–47.

Morgan, J.K., Moore, G.F., Hills, D.J., Leslie, S., 2000. Overthrusting and sediment accretion along Kilauea's mobile south flank, Hawaii: evidence for volcanic spreading from marine seismic reflection data. Geology 28, 667–670.

Morgan, J.K., Moore, G.F., Clague, D.A., 2003. Slope failure and volcanic spreading along the submarine south flank of Kilauea volcano, HI. J. Geophys. Res. 108, 2415.

Murray, M.H., Marshall, G.A., Lisowski, M., Stein, R.S., 1996. The 1992 M=7 Cape Mendocino, California, earthquake: coseismic deformation at the south end of the Cascadia megathrust. J. Geophys. Res. 101, 17707–17725.

Nettles, M., Ekstrom, G., 2004. Long-period source characteristics of the 1975 Kalapana, Hawaii, Earthquake. Bull. Seismol. Soc. Am. 94 (2), 422–429.

Okada, Y., 1985. Surface deformation due to shear and tensile faults in a half-space. Bull. Seismol. Soc. Am. 75, 1135–1154.

Okamura, A., 1988. Water-tube and spirit-level tilt data, Hawaiian Volcano Observatory. U.S.G.S. Open-File Rep. 88-238.

Okubo, P.G., Benz, H.M., Chouet, B.A., 1997. Imaging the crustal magma sources beneath Mauna Loa and Kilauea Volcanoes, Hawaii. Geology 25 (10), 867–870.

Owen, S., Bürgmann, R., 1999. Relationship of the 1974 southwest rift zone intrusion to the 1975 M7.2 Kalapana south flank earthquake on Kilauea Volcano [abs.]. Eos, Trans., Am. Geophys. Union Supp. 80 (47).

Owen, S., Segall, P., Freymueller, J., Miklius, A., Denlinger, R., Arnodottir, T., Sako, M., Bürgmannn, R., 1995. Rapid deformation of the south flank of Kilauea Volcano, Hawaii. Science 267, 1328–1332.

Owen, S.E., Segall, P., Lisowski, M., Miklius, A., Denlinger, R., Freymueller, J., Arnadottir, T., Sako, M., 2000. Rapid deformation of Kilauea Volcano: GPS measurements between 1990 and 1996. J. Geophys. Res. 105 (B8), 18983–18998.

Ryan, M.P., 1988. The mechanics and three-dimensional internal structure of active magmatic systems: Kilauea Volcano, Hawaii. J. Geophys. Res. 93, 4213–4248.

Ryan, M.P., Blevens, J.Y., Okamura, A.T., Koyanagi, R.Y., 1983. Magma reservoir subsidence mechanics: theoretical summary and application to Kilauea Volcano, Hawaii. J. Geophys. Res. 88 (B5), 4147–4181.

Segall, P., Mathews, M.V., 1988. Displacement calculations from geodetic data and the testing of geophysical deformation models. J. Geophys. Res. 93, 14954–14966.

Stark, P.B., Parker, R.L., 1995. Bounded-variable least-squares: an algorithm and applications. Comp. Stat. 10, 129–141.

Stearns, H.T., Macdonald, G.M., 1946. Geology and ground-water resources of the island of Hawaii. Hawaii (Terr.) Division of Hydrography Bulletin 9: 363 p.; 2 folded maps in pocket (scale 1:125 000) (includes plates).

Swanson, D.A., Duffield, W.A., Fiske, R.S., 1976. Displacement of the south flank of Kilauea Volcano: the result of forceful intrusion of magma into the rift zones. U. S. Geol. Surv. Prof. Pap. 963, 1–37.

Thurber, C.H., Gripp, A.E., 1988. Flexure and seismicity beneath the south flank of Kilauea Volcano and tectonic implications. J. Geophys. Res. 93, 4271–4278.

Tilling, R.I., et al., 1976. Earthquake and related catastropic events, island of Hawaii, November 29, l975: a preliminary report. U.S. Geol. Surv. Circ. 740, 33.

Wood, H.O., 1914. On the earthquakes of 1868 in Hawaii. Bull. Seismol. Soc. Am. 4, 169–203.

Wyss, M., 1988. A proposed source model for the great Kau, Hawaii, earthquake of 1868. Bull. Seismol. Soc. Am. 78, 1450–1462.

Wyss, M., Gillard, D., 1992. The role of normal faulting in large earthquakes along Hawaii's south-east coast ([abs.]). Eos, Trans., Am. Geophys. Union Supp. 73 (43), 506.

Wyss, M., Koyanagi, R.Y., 1992. Isoseismal maps, macroseismic epicenters, and estimated magnitudes of historical earthquakes in the Hawaiian Islands. U.S. Geol. Surv. Bull. 2006, 93.

Wyss, M., Koyanagi, R.Y., 1992. Seismic gaps in Hawaii. Bull. Seismol. Soc. Am. 82 (3), 1373–1387.

Wyss, M., Klein, F.W., Johnston, A.C., 1981. Precursors to the Kalapana $M=7.2$ earthquake. J. Geophys. Res. 86 (B5), 3881–3900.

Yang, X.-M., Davis, P.M., Dieterich, J.H., 1988. Deformation from inflation of a dipping finite prolate spheroid in an elastic half-space as a model for volcanic stressing. J. Geophys. Res. 93 (B5), 4249–4257.

Yang, X., Davis, P.M., Delaney, P.T., Okamura, A.T., 1992. Geodetic analysis of dike intrusion and motion of the magma reservoir beneath the summit of Kilauea Volcano, Hawaii. J. Geophys. Res. 97, 3305–3324.